



# Reactive nitrogen ( $\text{NO}_y$ ) and ozone responses to energetic electron precipitation during Southern Hemisphere winter

Pavle Arsenovic<sup>1,a</sup>, Alessandro Damiani<sup>2</sup>, Eugene Rozanov<sup>1,3,4</sup>, Bernd Funke<sup>5</sup>, Andrea Stenke<sup>1</sup>, and Thomas Peter<sup>1</sup>

<sup>1</sup>Institute for Atmospheric and Climate Science, ETH, Zürich, Switzerland

<sup>2</sup>Center for Environmental Remote Sensing (CEReS), Chiba University, Chiba, Japan

<sup>3</sup>Physikalisch-Meteorologisches Observatorium Davos – World Radiation Center, Davos, Switzerland

<sup>4</sup>Pushkov Institute of Terrestrial Magnetism, Ionosphere, and Radio Wave Propagation, Russian Academy of Sciences, Kaliningrad, Russia

<sup>5</sup>Instituto Astrofísica Andalucía, Consejo Superior de Investigaciones Científicas, Granada, Spain

<sup>a</sup>now at: Air Pollution/Environmental Technology, Empa, Dübendorf, Switzerland

**Correspondence:** Pavle Arsenovic (pavle.arsenovich@gmail.com)

Received: 23 October 2018 – Discussion started: 23 November 2018

Revised: 4 June 2019 – Accepted: 18 June 2019 – Published: 26 July 2019

**Abstract.** Energetic particle precipitation (EPP) affects the chemistry of the polar middle atmosphere by producing reactive nitrogen ( $\text{NO}_y$ ) and hydrogen ( $\text{HO}_x$ ) species, which then catalytically destroy ozone. Recently, there have been major advances in constraining these particle impacts through a parametrization of  $\text{NO}_y$  based on high-quality observations. Here we investigate the effects of low (auroral) and middle (radiation belt) energy range electrons, separately and in combination, on reactive nitrogen and hydrogen species as well as on ozone during Southern Hemisphere winters from 2002 to 2010 using the SOCOL3-MPIOM chemistry-climate model. Our results show that, in the absence of solar proton events, low-energy electrons produce the majority of  $\text{NO}_y$  in the polar mesosphere and stratosphere. In the polar vortex,  $\text{NO}_y$  subsides and affects ozone at lower altitudes, down to 10 hPa. Comparing a year with high electron precipitation with a quiescent period, we found large ozone depletion in the mesosphere; as the anomaly propagates downward, 15 % less ozone is found in the stratosphere during winter, which is confirmed by satellite observations. Only with both low- and middle-energy electrons does our model reproduce the observed stratospheric ozone anomaly.

## 1 Introduction

Energetic particles originating from the Sun, the magnetosphere, or outside the solar system continuously precipitate into the Earth's atmosphere and can influence atmospheric processes. They ionize neutral air molecules, especially in the middle and upper polar atmosphere, and create odd nitrogen and hydrogen species,  $\text{NO}_x$  ( $[\text{N}] + [\text{NO}] + [\text{NO}_2]$ ) and  $\text{HO}_x$  ( $[\text{H}] + [\text{OH}] + [\text{HO}_2]$ ).  $\text{NO}_x$  and  $\text{HO}_x$  radicals can catalytically deplete ozone. The in situ destruction of ozone in the mesosphere is characteristic of  $\text{HO}_x$  due to its fast reaction rates (Bates and Nicolet, 1950). On the other hand,  $\text{NO}_x$ , in the absence of sunlight, subsides within the downwelling branch of the overturning circulation, affecting ozone concentrations at lower altitudes (Solomon et al., 1982).

High-energy particles, i.e. solar protons (Jackman et al., 2008) and radiation belt electrons (Arsenovic et al., 2016; Semeniuk et al., 2011), can penetrate directly into the mesosphere and stratosphere. Radiation belt electrons (energies  $> 30$  keV) impact chemistry below 90 km in the atmosphere (Turunen et al., 2009). Electrons of lower energies ( $< 30$  keV, auroral) originate from the magnetosphere as well as the radiation belt electrons (Mironova et al., 2015), but they get accelerated in the magnetotail and precipitate into the lower thermosphere in the auroral ovals ( $55$ – $70^\circ$  geomagnetic latitude) (Baker et al., 2001; Barth et al., 2003). Their peak impact is above 90 km in the thermosphere (Turunen et al., 2009).

There have been numerous attempts to include low-energy electrons (LEE) in climate models. Chemistry-climate or chemistry-transport models with top in the thermosphere, e.g. HAMMONIA (Schmidt et al., 2006), KASIMA (Reddmann et al., 2010), and WACCM (Andersson et al., 2018; Marsh et al., 2007), have included effects of LEE directly because they deposit their energy within the model domain. For climate models that have an upper lid below the thermosphere, a prescription of LEE either as NO<sub>y</sub> influx through the model top or as concentrations (number density) in the upper model boxes is recommended (Matthes et al., 2017). Baumgaertner et al. (2009) developed a parameterization of this flux based on the geomagnetic activity A<sub>p</sub> index, a daily worldwide measure of the effects of solar wind on the Earth's magnetic field. When incorporated into a chemistry-climate model, results showed significant ozone depletion in the mesosphere and stratosphere (Baumgaertner et al., 2011). For the SOCOL chemistry-climate model, Rozanov et al. (2012) also found significant ozone decreases in the mesosphere and stratosphere, with peak values around 10 % in September around 36 km altitude over the Antarctic.

Funke et al. (2016) recently developed a semi-empirical model that calculates concentrations and fluxes of mesospheric and stratospheric NO<sub>y</sub> compounds ([NO] + [NO<sub>2</sub>] + 2 × [N<sub>2</sub>O<sub>5</sub>] + [HNO<sub>3</sub>] + [ClONO<sub>2</sub>]) based on the Michelson Interferometer for Passive Atmospheric Sounding (MIPAS) observations. The model exploits the nearly linear relationship in the mesosphere between the A<sub>p</sub> index with observed NO<sub>y</sub> produced by EPP. This advance in the representation of LEE in climate models motivates us to investigate whether LEE can have a larger impact on atmospheric chemistry than previously thought (Rozanov et al., 2012). Moreover, this LEE parameterization is a part of the recommended solar forcing dataset for climate models within the upcoming Coupled Model Intercomparison Project Phase 6 (CMIP-6, Matthes et al., 2017).

It is crucial to have a realistic representation of EPP in models as the introduced signal impacts atmospheric chemistry and potentially regional climate (Baumgaertner et al., 2011; Maliniemi et al., 2014; Rozanov et al., 2012; Seppälä et al., 2013). Sinnhuber et al. (2018) showed the impact of one possible implementation of the new Funke et al. (2016) LEE NO<sub>y</sub> parameterization in their EMAC model on NO<sub>y</sub> and ozone; however, they did not explicitly consider MEE. Here we present results from our state-of-the-art chemistry-climate model, employing a different implementation of the same parameterization of LEE together with the previous representations of other energetic particles. This paper focuses on evaluating NO<sub>x</sub> and ozone response to LEE and MEE precipitation, separately and in combination, in Antarctic winters (JJA: June, July, and August), in order to avoid the more complicated Arctic polar vortex with its high variability and strong dependence on meteorological conditions (Hitchcock et al., 2013). We compare our results with the satellite observations.

## 2 Methods

We used the SOCOL3-MPIOM coupled chemistry-climate model (Muthers et al., 2014; Stenke et al., 2013). The atmospheric dynamic component of the model is ECHAM5.4 (Roeckner and Bäuml, 2003), coupled to the MEZON air chemistry module (Egorova et al., 2003; Rozanov et al., 1999) and the MPIOM interactive ocean module (Jungclaus et al., 2006; Marsland et al., 2002). We carried out the experiments with T31 spectral resolution on 39 vertical levels from the surface up to 0.01 hPa (~ 80 km).

The model boundary conditions and parameterizations are identical to those described in Arsenovic et al. (2016), except for the LEE parameterization. Following Calisto et al. (2011), galactic cosmic rays (GCR) are parameterized as a function of geomagnetic latitude, pressure, and solar modulation potential. Ionization by solar protons (SP) is treated according to Jackman et al. (2008) and ionization by middle-energy electrons (MEE) with energies between 30 and 300 keV is taken from the Atmospheric Ionization Module Osnabrück (AIMOS) v1.6 (Arsenovic et al., 2016; Wissing and Kallenrode, 2009). Electrons of energies higher than 300 keV are not included in the model due to a lack of adequate parameterization.

For LEE, we are using the semi-empirical model for NO<sub>y</sub> influx by Funke et al. (2016) through the model top at 0.01 hPa (75–80 km in polar conditions). Although MIPAS scans the atmosphere up to 68 km altitude, the applicability of this parameterization above 70 km has been validated by comparison with MIPAS middle- and upper-atmosphere observations (scanning up to 100 and 170 km, respectively). As more than 99 % of the NO<sub>y</sub> at this altitude is in the form of nitrogen monoxide (nitric oxide), NO (Brasseur and Solomon, 2005), we approximate the NO<sub>y</sub> influx calculated by the semi-empirical model as NO influx at this level in SOCOL3-MPIOM. As mentioned before, LEE precipitate above 90 km and MEE precipitate between 70 and 90 km altitude (Turunen et al., 2009). However, because of our model top at 80 km, here we consider electrons that precipitate below 80 km to be MEE and electrons that precipitate above the model top to be LEE.

Matthes et al. (2017) and Sinnhuber et al. (2018) also implemented the parameterization by Funke et al. (2016) in the EMAC model. They used a different approach, prescribing NO concentrations (instead of fluxes through the model top) in the model within the 0.09–0.01 hPa layer and performed the simulations with specified dynamics. Prescribing concentrations requires overwriting NO simulated values. It is inconsistent with the treatment of the physical and chemical processes in our model leading to accumulation of NO<sub>y</sub>. This is not the case for the influx approach and therefore we prescribe the NO influx instead of NO concentrations; however, prescribed NO concentrations can be used for models with different treatments of the chemical and transport processes.

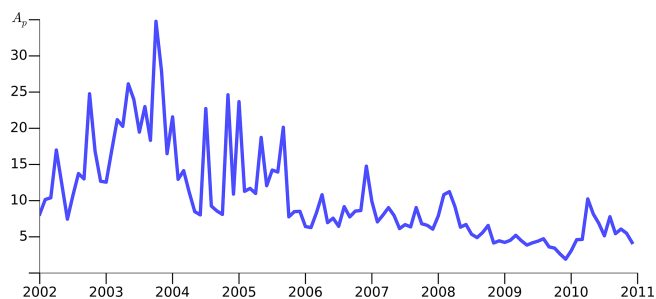


**Figure 1.** The monthly mean geomagnetic  $A_p$  index during the simulated period: years 2002–2005 were rather active, while the period 2006–2010 was geomagnetically quiescent (CMIP-6 dataset; Matthes et al., 2017).

Figure 1 shows the monthly mean geomagnetic  $A_p$  index that covers our simulated period. Period 2002–2005 was characterized by a rather high  $A_p$  index and the 2006–2010 period by low values. For our simulations, we have used daily  $\text{NO}$  fluxes calculated from daily  $A_p$  indices.

Four sets of six-member ensemble simulations were carried out, covering the 2002–2010 period: the “ALL” simulation, which includes all energetic particles (GCR, SP, MEE, and LEE), the “LEE” simulation (GCR, SP, and LEE), the “MEE” simulation (GCR, SP, and MEE), and the reference “REF” simulation (GCR and SP). All these simulations have the same model boundary conditions and differ only in the inclusion of the low-/middle-energy electron precipitation.

We used two satellite datasets to evaluate our model results: MIPAS for nitrogen species and the Microwave Limb Sounder (MLS) for ozone. MIPAS was a Fourier transform spectrometer aboard the ENVISAT satellite (Fischer et al., 2008). The quality of MIPAS  $\text{NO}_y$  and individual  $\text{NO}_y$  species has been extensively assessed in SPARC (2017), as well as specific validation studies (e.g. Bender et al., 2015; Sheese et al., 2016). The top altitude of the MIPAS nominal limb scans is 68 km, but it also contains information on the  $\text{NO}_y$  above, though with low vertical resolution. Since it provides the entire  $\text{NO}_y$  budget in the upper atmosphere (with a vertical resolution of 3–5 km), we used this dataset to validate simulated  $\text{NO}_y$ .

The MLS aboard the Aura satellite (Waters et al., 2006) has provided daily measurements of ozone profiles (Froidevaux et al., 2008) in the middle and upper atmosphere since August 2004. We used MLS observations to evaluate modelled ozone. The vertical resolution of MLS  $\text{O}_3$  (v4.2) is about 3 km in the stratosphere, increasing up to about 5 km in the mesosphere (Livesey et al., 2018).

## 3 Results

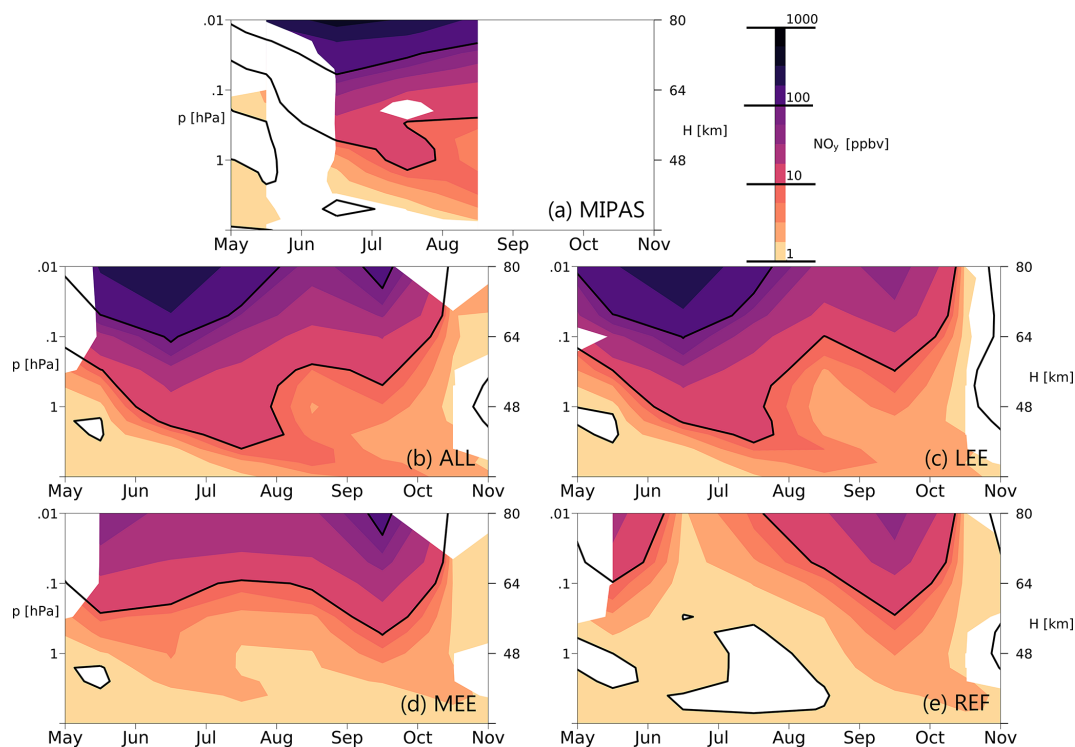
### 3.1 $\text{NO}_y$ enhancement propagation

Figure 2 shows the difference in  $\text{NO}_y$  concentration between the geomagnetically active year 2005 and the mean over the geomagnetically quiescent period 2006–2010 averaged over 70–90° S. Even though year 2003 on average has higher  $A_p$ , here we choose year 2005 as the geomagnetically active year. This allows us to compare modelled  $\text{NO}_y$  and ozone using two different satellite datasets, MIPAS and MLS (which have been available only since 2005). MIPAS data are unavailable from September 2005 to the end of the year, but our main period of interest is JJA, which is well covered by the observations.

The MIPAS observations (Fig. 2a) show a  $\text{NO}_y$  enhancement throughout the mesosphere and upper stratosphere. In terms of mixing ratio, the highest increase of 500–600 ppbv is found in the upper mesosphere around 0.01 hPa ( $\sim 80$  km). There, the highest monthly values are observed in June. In the following months, this anomaly descends and reaches lower levels. In July, the  $\text{NO}_y$  enhancement of around 10 ppbv reaches the upper stratosphere around 2 hPa, and the increase, although smaller, is visible all the way down to 10 hPa. In the following months, the MIPAS nominal data were unavailable due to special observation mode campaigns.

The ALL experiment (Fig. 2b) shows a very similar pattern of  $\text{NO}_y$  to the observations. The  $\text{NO}_y$  increase of 500–600 ppbv in the upper mesosphere around 0.01 hPa is similar to the MIPAS observations. However, the wintertime  $\text{NO}_y$  peak below is slightly overestimated in the model compared to MIPAS. This is particularly visible in the lower mesosphere in June, as the modelled 100 ppbv  $\text{NO}_y$  enhancement reaches 0.1 hPa. The mesospheric anomaly extends into the stratosphere, but remains confined to the upper stratosphere, above 10 hPa, as in observations. The modelled  $\text{NO}_y$  overestimation suggests that downward transport is somewhat too fast in the model, or that the photochemical lifetime of  $\text{NO}_y$  is too long, or that horizontal mixing with mid-latitudes is underestimated. The modelled  $\text{NO}_y$  enhancement in September stems from an SP event (NOAA). In contradiction to our results, the EMAC model slightly underestimates  $\text{NO}_y$  even during polar summer, for two pressure levels, 0.1 and 1 hPa (Matthes et al., 2017). Sinnhuber et al. (2018) showed underestimation of  $\text{NO}_y$  in the upper mesosphere in the EMAC and KASIMA models and overestimation of  $\text{NO}_y$  in the 3dCTM model in the Southern Hemisphere compared to MIPAS observations.

The LEE simulation (Fig. 2c) shows very similar anomalies to ALL. The largest differences are in the upper mesosphere, where LEE anomalies reach around 400 ppbv, which is underestimated compared to the 500–600 ppbv found in MIPAS and ALL. A second interesting difference compared to ALL is the SP event in September. In the LEE simulation,



**Figure 2.** Monthly mean  $\text{NO}_y$  volume mixing ratio anomaly in ppbv for the Southern Hemisphere ( $> 70^\circ \text{S}$  average) calculated as the difference of the year 2005 and the average of 2006–2010. (a) MIPAS observations; (b) ensemble mean of ALL simulations; (c) ensemble mean of LEE simulations; (d) ensemble mean of MEE simulations; (e) ensemble mean of REF simulations. Colour levels are 1, 2.5, 5, 7.5, 10, 25, 50, 75, 100, 250, 500, 750, and 1000 ppbv and the black contour lines highlight 1, 10, 100, and 1000 ppbv. Coloured regions are significant at the 99 % confidence level (calculated using a Student's  $t$  test).

it reaches around 60 ppbv, while in ALL it exceeds 100 ppbv. This difference comes from increased MEE precipitation that coincided with the SP event (see Arsenovic et al., 2016, Fig. 1a). During strong SP events protons can contaminate the highest electron channel, so this channel is excluded from the AIMOS dataset (Yando et al., 2011). Although some degree of contamination is still possible in the lower channels, protons are not the sole cause of the increased  $\text{NO}_y$  in this SP event. That is, SP events are often associated with large coronal mass ejections that form a shock in front of them. Once the shock hits the Earth it often leads to a geomagnetic storm which leads to acceleration of electrons of  $> 30 \text{ keV}$  energies. Therefore, increased MEE precipitation often happens very shortly after an SP event because the shock and the geomagnetic storm are related to the same coronal mass ejection driver (Asikainen and Ruopsa, 2016).

The MEE simulation (Fig. 2d) is drastically different from MIPAS as well as the ALL and LEE simulations. Although  $\text{NO}_y$  enhancement in the modelled geomagnetically active year exists, it is significantly decreased compared with the previous results. The modelled  $\text{NO}_y$  mesospheric anomaly peak is absent and enhancement of 10 ppbv does not reach the stratosphere. Nevertheless, although less intense, increased  $\text{NO}_y$  is present throughout the mesosphere

and stratosphere, and the  $\text{NO}_y$  increase in September due to the SP event again exceeds 100 ppbv, as in the ALL simulation.

The reference run in Fig. 2e shows  $\text{NO}_y$  increase due to the SP events in the year 2005. In this year, there were six observed SP events in the shown time frame – 14 May, 16 June, 14 and 27 July, 22 August, and 8 September (NOAA). In the geomagnetically inactive period, 2006–2010, there were no observed SP events in the presented months. Therefore, by excluding electron precipitation, the SP events alone cannot reproduce the observed features.

From the presented months, we conclude that the inclusion of only LEE was sufficient to reproduce most of the  $\text{NO}_y$  enhancements. The MEE contribution to  $\text{NO}_y$  increases is minor and brings the model closer to observations mainly in the upper mesosphere. As coronal mass ejections drive SP events and they can have an impact on the precipitation from the outer Van Allen belt (Asikainen and Ruopsa, 2016; Pierrard and Lopez Rosson, 2016), MEE precipitation could significantly contribute to  $\text{NO}_y$  increases in such events.

### 3.2 O<sub>3</sub> anomaly propagation

In the study of Matthes et al. (2017), ozone responses were evaluated by comparing high and low geomagnetic activity years, and their estimate shows good agreement with satellite observations (Fytterer et al., 2015). To evaluate our simulated ozone responses, we follow a similar approach to that used in Matthes et al. (2017); that is, we compared our simulations with observations from MLS. We analysed the 2005–2010 period when both simulation and MLS data are available.

Ozone anomalies from MLS observations during the high geomagnetically active year are depicted in Fig. 3a. They are calculated as the difference averaged over 70–90° S between the active year (2005) and the average of geomagnetically quiet years (2006–2010) divided by the ozone averaged over the whole period (2005–2010). Observations show around 20 % less ozone in the upper mesosphere (< 0.1 hPa) occurring mostly in the JJA period. The exception is the SP event on 8 September 2005. It created an ozone anomaly of up to 80 % stretching throughout the whole mesosphere. The mesosphere below 0.1 hPa does not show a statistically significant difference between the geomagnetically active and quiet years in the absence of SP events. The observed negative ozone anomaly appears again around the stratopause in late June and propagates downwards to nearly 10 hPa in early September. The peak ozone anomaly occurs in August around 3 hPa, reaching ~ 15 %. Our results agree with the results from previous modelling studies (Reddmann et al., 2010; Rozanov et al., 2012; Sinnhuber et al., 2018) and observations (Damiani et al., 2016; Fytterer et al., 2015).

The ALL simulation (Fig. 3b) shows a negative ozone anomaly in the mesosphere as well. However, the magnitude is generally higher (around 30 %), and it is present from May to September. The September 2005 SP event is visible in the model simulations as well and descends from around 1 hPa in late September, reaching 10 hPa in late October. A similar pattern, but less obvious, is seen in the observations. Ozone anomalies in the lower mesosphere (0.5–0.1 hPa) are more pronounced in the model than in MLS observations. This is particularly evident in June when the modelled upper-mesosphere anomaly appears to relate to the upper-stratospheric anomaly, in contrast to the observations. This suggests that HO<sub>x</sub> production by MEE might be overestimated. In the upper stratosphere model simulations agree well with observations. The decrease propagates downwards, reaching approximately 10 hPa in August, with a peak around 15 % in good agreement with the observations.

Ozone anomalies in the LEE simulation are shown in Fig. 3c. Negative ozone anomalies are present mostly in the upper mesosphere (above 0.3 hPa) and have similar magnitude to ALL. Although in the LEE simulation the mesospheric ozone anomaly is overestimated compared to MLS observations, the stratospheric anomaly is almost completely absent. This is surprising, as there are very similar NO<sub>y</sub> anomalies in the ALL and LEE simulations (see Fig. 2).

Our MEE simulation shows similar ozone anomalies compared to LEE (Fig. 3d). The anomalies are confined to a region above 1 hPa and are somewhat reduced compared to LEE and ALL. Similar to LEE, the stratospheric ozone anomaly seen in the observations and ALL simulation is almost absent.

In REF simulation (Fig. 3e) most of the ozone anomaly features seen in observations and ALL are missing. The only depletion of ozone in this simulation is caused by SP events in the year 2005. Most of the observed events (14 May, 16 June, 14 and 27 July, 22 August, and 8 September) are clearly visible.

A recent study based on CCM WACCM (Andersson et al., 2018) showed ozone anomaly propagation differences between high-*A<sub>p</sub>* and low-*A<sub>p</sub>* winters in the Southern Hemisphere. Their results are comparable with our ALL and LEE simulations. Compared with our ALL simulation, their ozone anomaly in the case of all EEP of around 7 % is lower and occurs later (in October as opposed to August). However, their LEE simulation does not show a significant ozone anomaly in the stratosphere, which is also the case in our results. In the study of Sinnhuber et al. (2018) the three analysed models (3dCTM, KASIMA, and EMAC) generally show good agreement with the satellite observations.

### 3.3 EEP effect on NO<sub>y</sub>, HO<sub>x</sub>, and O<sub>3</sub>

To estimate the total effect of energetic electron precipitation on NO<sub>y</sub>, HO<sub>x</sub>, and ozone, we calculated the differences of experiment simulations (ALL, LEE, and MEE) and REF simulation for the geomagnetically active period (2002–2005) using the simulated monthly mean values. Note that this is an idealized comparison and it is not directly comparable with observations, as there is always some amount of particle precipitation in the atmosphere (Funke et al., 2014), unlike in the LEE, MEE, and REF simulations.

The zonal mean of austral winter (JJA) average NO<sub>y</sub> differences between ALL and REF is shown in Fig. 4a. In polar night, NO<sub>y</sub> is transported to lower altitudes by descending air motion. Significant modelled NO<sub>y</sub> enhancements are present in the whole mesosphere and upper stratosphere above 10 hPa. Around 0.01 hPa, EPP produced NO<sub>y</sub> increases from 50 ppbv at around 60° S, where NO<sub>y</sub> lifetime is decreased due to the sunlight, to more than 500 ppbv at the pole, in the polar night. The differences in HO<sub>x</sub> between those two experiments are shown in Fig. 4b. Increases are mostly confined to the upper mesosphere and they reach the maximum of around 5 ppbv. However, smaller (< 1 ppbv) but statistically significant HO<sub>x</sub> increase appears in the lower mesosphere and upper stratosphere around 60° S. Increases in NO<sub>y</sub> and HO<sub>x</sub> impact the ozone chemistry. Figure 4c shows changes in ozone concentrations due to electron precipitation. Ozone is significantly reduced throughout the whole polar region above 10 hPa. There are two peaks of ozone anomaly. The maximum decrease of up to 65 % (350–

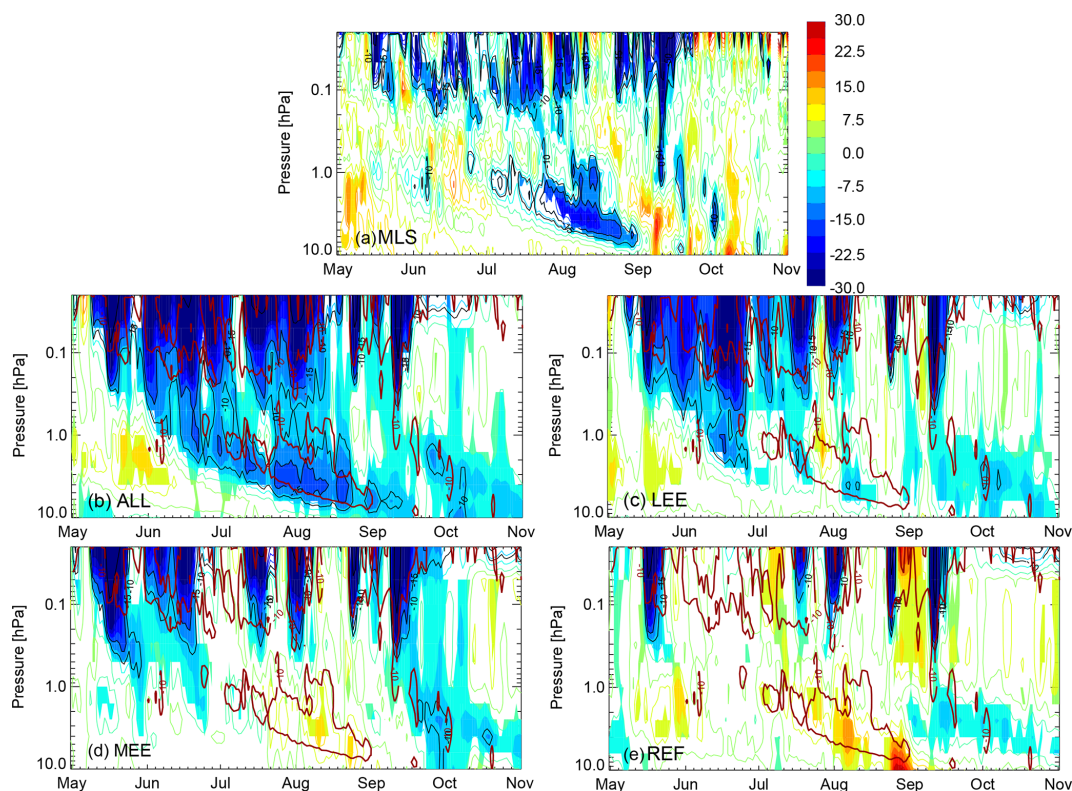


**Figure 3.** Monthly mean ozone anomaly poleward of  $70^\circ$  S calculated as the difference of year 2005 and average of 2006–2010 relative to the 2005–2010 period. (a) MLS observations; (b) ensemble mean of ALL simulations; (c) ensemble mean of LEE simulations; (d) ensemble mean of MEE simulations; (e) ensemble mean of REF simulations. Black lines highlight  $-10\%$ ,  $-15\%$ , and  $-50\%$  and dark red lines mark  $-10\%$  from MLS observations on every plot. Note that mesospheric ozone depletion reaches  $80\%$ – $90\%$  during some strong solar proton events. Coloured regions are significant at the  $99\%$  confidence level (calculated using a Student's  $t$  test).

400 ppbv) is located in the upper mesosphere. This decrease is more severe than in previous modelling studies (Rozanov et al., 2012), but this is because we focus on the geomagnetically active winters, when EPP effects are much more pronounced. The magnitude of ozone depletion is gradually decreasing with height, reaching  $\sim 15\%$  ( $> 200$  ppbv) at the stratopause. The second ozone depletion peak is located between 10 and 1 hPa, reaching  $15\%$  ( $> 400$  ppbv). A similar ozone response to ALL has been shown by Semeniuk et al. (2011).

Figure 4d shows the difference between modelled  $\text{NO}_y$  in LEE and REF simulation. Similarly, as in Fig. 2, modelled  $\text{NO}_y$  in LEE simulation is very similar to ALL, confirming the fact that most of the  $\text{NO}_y$  is coming from LEE. Slight reduction to ALL still exists, visible mostly at 0.1 hPa at  $90^\circ$  S. Here, the value of  $\text{NO}_y$  is 100 ppbv, while it is somewhat more in Fig. 4a. A second difference is the absence of the enhancement equatorward of  $30^\circ$  S which is present in Fig. 4a. Increase in  $\text{HO}_x$  in the case of LEE is illustrated in Fig. 4e. Changes in  $\text{HO}_x$  are very small and statistically insignificant, except for a small ( $< 1$  ppbv) increase in the polar upper mesosphere. This is expected as LEE do not produce  $\text{HO}_x$ . The small increase could be explained by an increase in  $\text{NO}_y$

which causes small increases in background  $\text{HO}_x$  through the Verronen and Lehmann (2015) mechanism, where enhanced NO coming from EEP leads to  $\text{HO}_x$  repartitioning increasing  $\text{HO}_x$  concentrations. Figure 4f shows ozone changes due to the LEE. A similar ozone decrease pattern to Fig. 4c exists but with a reduced intensity. The upper-mesospheric reduction reaches  $35\%$  ( $\sim 200$  ppbv) and the upper-stratospheric anomaly is halved compared to ALL ( $200$  ppbv  $\hat{=} 10\%$ ).  $\text{HO}_x$  increases and reduced ozone anomalies compared to ALL illustrate the importance of MEE.

Figure 4g shows an increase in  $\text{NO}_y$  due to the MEE. Although MEE cause increases in  $\text{NO}_y$ , modelled  $\text{NO}_y$  is significantly reduced in the whole area compared to LEE and ALL simulation. In the upper mesosphere, this increase is around 50 ppbv, or a tenth of the total produced  $\text{NO}_y$  in ALL simulation. Between  $30$  and  $35^\circ$  S  $\text{NO}_y$  enhancement is present again, as in ALL simulation. This enhancement is coming from the fact that MEE do not necessarily precipitate inside the polar vortex, as they precipitate in the sub-auroral ovals, which are centered around the geomagnetic pole. In contrast,  $\text{NO}_y$  coming from LEE descends into the mesosphere in the downwelling air motion inside of the polar vor-

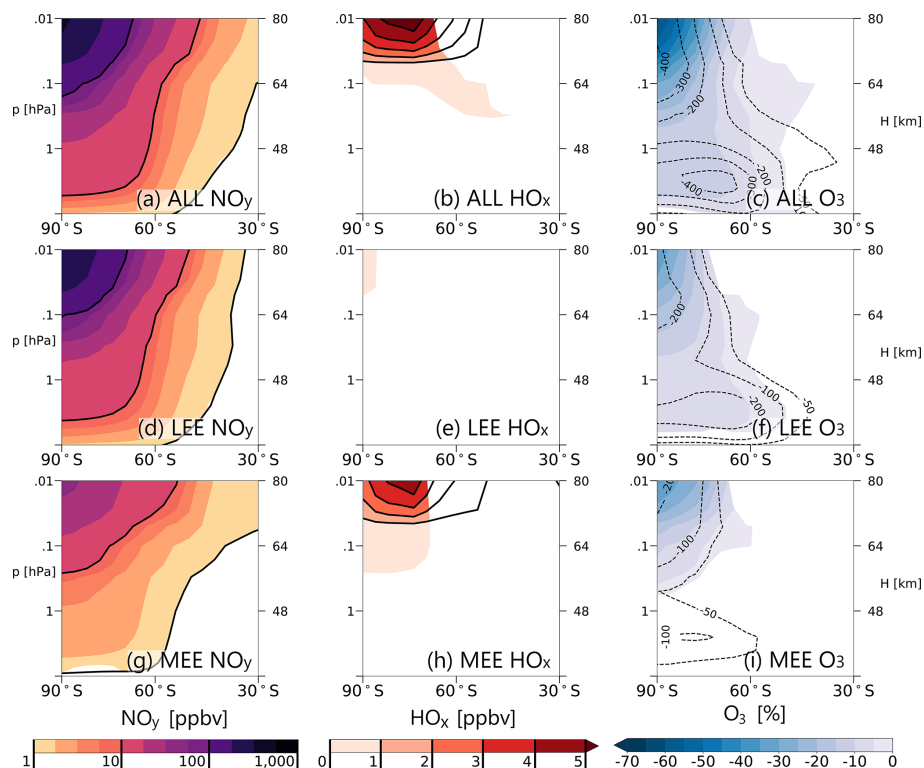


**Figure 4.** Summary of zonally averaged results. Columns: NO<sub>y</sub> (a, d, g); HO<sub>x</sub> (b, e, h); O<sub>3</sub> (c, f, i). Rows: including ALL energetic particles (a–c); only with LEE (d–f); only with MEE (g–i). All panels show results for the geomagnetically active period (2002–2005) for austral winter (JJA) from the respective simulations minus the REF simulation. Colours show absolute differences in ppbv for NO<sub>y</sub> (colour levels are 1, 2.5, 5, 7.5, 10, 25, 50, 75, 100, 250, 500, 750, and 1000 ppbv) and HO<sub>x</sub> plots and difference in percent for O<sub>3</sub> plots. Isolines show difference in absolute values in ppbv. Coloured regions are significant at the 99 % confidence level (calculated using a Student's *t* test).

tex. The sum of NO<sub>y</sub> increases (not shown) due to the LEE (Fig. 4d) and due to the MEE (Fig. 4g) closely reassembles NO<sub>y</sub> increase as in the ALL case (Fig. 4a).

Increases in HO<sub>x</sub> due to MEE are presented in Fig. 4h. Enhancements are present mostly in the upper mesosphere, reaching 4 ppbv. The position and intensity of HO<sub>x</sub> are very similar to ALL, but are somewhat reduced. Because MEE produce OH, neglecting MEE in climate models would lead to an underestimation of HO<sub>x</sub>; neglecting LEE would also lead to an underestimation of HO<sub>x</sub> through the changed HO<sub>x</sub> partitioning (Verronen and Lehmann, 2015). Changes in ozone concentrations due to MEE are shown in Fig. 4i. Negative ozone anomalies are present in the mesosphere and in the upper stratosphere, albeit the stratospheric anomaly is statistically not significant. The biggest reduction with 35 % (~ 200 ppbv) is visible in the upper mesosphere. The anomaly in the upper stratosphere (10–1 hPa) does not exceed 100 ppbv. Interestingly, summing stratospheric ozone anomaly from LEE (Fig. 3f) and from MEE (Fig. 3i) does not reproduce ALL ozone anomaly (Fig. 3c). The sum of the LEE and MEE ozone anomaly accounts for around 300 ppbv, while ALL shows about 400 ppbv between 10 and 1 hPa. Since the sum of enhanced NO<sub>y</sub> due to LEE and MEE cor-

responds to ALL NO<sub>y</sub> and HO<sub>x</sub> enhancements occur in the mesosphere, this discrepancy in ozone anomaly cannot be chemically explained. It could be caused by changes in dynamics (polar vortex strength) and temperature (which affects reaction rates).

Our results indicate that LEE and MEE are equally responsible for the ozone anomaly in the mesosphere. LEE deplete ozone through the production of large amounts of NO<sub>y</sub>, while MEE contribute to the anomaly mostly through production of HO<sub>x</sub>, which is the more efficient ozone destructor (Brasseur and Solomon, 2005). Both LEE and MEE produce the stratospheric anomaly; however, LEE, through the production of large amounts of NO<sub>y</sub>, are more important.

## 4 Conclusions

We used the period 2005–2010 comprising intervals of high and low geomagnetic activity, which is well characterized by stratospheric and mesospheric measurements of NO<sub>y</sub> and O<sub>3</sub>, to investigate the accuracy of representations of energetic particle forcing in a chemistry-climate model. We assessed the impact of employing a new parameterization of LEE (< 30 keV) recommended for CMIP-6 in combination

with the AIMOS parameterization for MEE (30–300 keV) on the simulated NO<sub>y</sub>, HO<sub>x</sub>, and ozone variability. We used the SOCOL3-MPIOM climate model and focused on the Southern Hemispheric winter season. We compared NO<sub>y</sub> with stratospheric and mesospheric MIPAS observations. The model captures the main features very well, but shows some differences in the winter maxima. LEE can reproduce most of the NO<sub>y</sub> features, without including MEE. However, increased MEE precipitation coincident with SP events may be a significant contribution to the observed NO<sub>y</sub> amounts.

Simulated ozone depletion has been compared to MLS satellite observations, showing that patterns of ozone anomalies during the high EPP year 2005 compared to 2006–2010 match reasonably well. The model overestimates mesospheric ozone anomalies, but in the stratosphere a good match is accomplished. Ozone depletion of up to 15 % is found during July and August and reaches into the lower stratosphere. In essence, without including both LEE and MEE, the stratospheric anomaly cannot be accurately modelled. Future work is required to address the roles of indirect changes in temperature and dynamics in the EPP-induced stratospheric ozone variation.

Most of the NO<sub>y</sub> in the mesosphere and stratosphere is produced by LEE in the upper mesosphere and lower thermosphere (< 0.01 hPa) and transported downwards. A smaller fraction, namely ~ 10 %, is generated in situ by ionization due to precipitating electrons of higher energies. These electrons play an important role because they produce HO<sub>x</sub>, which depletes ozone near the HO<sub>x</sub> source region in the mesosphere. Although not producing HO<sub>x</sub> directly, LEE increase NO<sub>y</sub> concentrations, which then causes repartitioning of HO<sub>x</sub> and an increase in the HO<sub>x</sub> lifetime (Verronen and Lehmann, 2015).

In summary, LEE and MEE lead to a reduction of ozone throughout the mesospheric and stratospheric polar region, with a maximum percentage ozone depletion in the mesosphere (–65 %) and a second peak anomaly in the upper stratosphere (–15 %) with respect to the simulation where they are omitted. These chemical EPP signals can cause dynamical changes in the stratosphere that propagate into the lower atmosphere, which eventually affect regional climate (Rozanov et al., 2012). Therefore, we recommend including both LEE and MEE in climate models.

**Data availability.** Due to the size limitations, SOCOL3-MPIOM model code, model boundary conditions, and satellite data are only available upon request. The model output analysed in this study can be found at <https://data.mendeley.com/datasets/kgzwjgf4bk/1> (<https://doi.org/10.17632/kgzwjgf4bk.1>, Arsenovic, 2019).

**Author contributions.** PA and ER proposed the idea and designed the experiments; PA carried out the simulations and prepared the manuscript. AD analysed MLS data and made Fig. 3. BF provided

MIPAS data. TP formulated the general line of research and supervised the project. All authors provided critical feedback and helped shape the research, analysis, and manuscript.

**Competing interests.** The authors declare that they have no conflict of interest.

**Acknowledgements.** This work is a part of ROSMIC WG1 activity within the SCOSTEP VarSITI programme and WG3 and 5 activities within the SPARC SOLARIS-HEPPA project. The authors thank NASA Goddard Earth Science Data and Information Services Center (GES DISC) for providing Aura/MLS data (<https://mls.jpl.nasa.gov/>, last access: 4 July 2019), Timo Asikainen (University of Oulu) for clarification of the MEE–SP events relationship, Marina Dütsch (University of Washington) and Jelisaveta Arsenovic for assistance with improving the graphics, and Amewu Mensah (ETH, Zürich) and William Ball (PMOD/WRC, Davos, and ETH, Zürich) for correcting the language. We thank our editor, Gabriele Stiller, Svenja Lange, and three anonymous reviewers whose comments significantly improved the quality of this paper.

**Financial support.** This research has been supported by the Swiss National Science Foundation (grant no. CRSII2-147659), the FONDECYT (grant no. 1171690), the MCINN (grant no. ESP2014-54362-P), the JST/CREST/EMS/TEEDDA (grant JPMJCR15K4), the EC FEDER, and the Russian Science Foundation (grant no. 17-17-01060).

**Review statement.** This paper was edited by Gabriele Stiller and reviewed by three anonymous referees.

## References

- Andersson, M. E., Verronen, P. T., Marsh, D. R., Seppälä, A., Päiväranta, S. M., Rodger, C. J., Clilverd, M. A., Kalakoski, N., and van de Kamp, M.: Polar Ozone Response to Energetic Particle Precipitation Over Decadal Time Scales: The Role of Medium-Energy Electrons, *J. Geophys. Res.-Atmos.*, 123, 607–622, <https://doi.org/10.1002/2017JD027605>, 2018.
- Arsenovic, P.: SOCOL3-MPIOM model output, Mendeley Data, v1, <https://doi.org/10.17632/kgzwjgf4bk.1>, 2019.
- Arsenovic, P., Rozanov, E., Stenke, A., Funke, B., Wissing, J. M., Mursula, K., Tummon, F., and Peter, T.: The influence of Middle Range Energy Electrons on atmospheric chemistry and regional climate, *J. Atmos. Sol.-Terr. Phys.*, 149, 180–190, <https://doi.org/10.1016/j.jastp.2016.04.008>, 2016.
- Asikainen, T. and Ruoposa, M.: Solar wind drivers of energetic electron precipitation, *J. Geophys. Res.-Space*, 121, 2209–2225, <https://doi.org/10.1029/2002JA009458>, 2016.
- Baker, D. N., Barth, C. A., Mankoff, K. E., Kanekal, S. G., Bailey, S. M., Mason, G. M., and Mazur, J. E.: Relationships between precipitating auroral zone electrons and lower thermospheric ni-

- tric oxide densities: 1998–2000, *J. Geophys. Res.*, 106, 24465–24480, <https://doi.org/10.1029/2001JA000078>, 2001.
- Barth, C. A., Mankoff, K. D., Bailey, S. M., and Solomon, S. C.: Global observations of nitric oxide in the thermosphere, *J. Geophys. Res.-Space*, 108, 1–11, <https://doi.org/10.1029/2002JA009458>, 2003.
- Bates, D. and Nicolet, M.: The photochemistry of atmospheric water vapor, *J. Geophys. Res.*, 55, 301–327, <https://doi.org/10.1029/JZ055i003p00301>, 1950.
- Baumgaertner, A. J. G., Jöckel, P., and Brühl, C.: Energetic particle precipitation in ECHAM5/MESSy1 – Part 1: Downward transport of upper atmospheric NO<sub>x</sub> produced by low energy electrons, *Atmos. Chem. Phys.*, 9, 2729–2740, <https://doi.org/10.5194/acp-9-2729-2009>, 2009.
- Baumgaertner, A. J. G., Seppälä, A., Jöckel, P., and Clilverd, M. A.: Corrigendum to “Geomagnetic activity related NO<sub>x</sub> enhancements and polar surface air temperature variability in a chemistry climate model: modulation of the NAM index” published in *Atmos. Chem. Phys.*, 11, 4521–4531, 2011, *Atmos. Chem. Phys.*, 11, 4687–4687, <https://doi.org/10.5194/acp-11-4687-2011>, 2011.
- Bender, S., Sinnhuber, M., von Clarmann, T., Stiller, G., Funke, B., López-Puertas, M., Urban, J., Pérot, K., Walker, K. A., and Burrows, J. P.: Comparison of nitric oxide measurements in the mesosphere and lower thermosphere from ACE-FTS, MIPAS, SCIAMACHY, and SMR, *Atmos. Meas. Tech.*, 8, 4171–4195, <https://doi.org/10.5194/amt-8-4171-2015>, 2015.
- Brasseur, G. P. and Solomon, S.: *Aeronomy of the middle atmosphere: Chemistry and physics of the stratosphere and mesosphere*, Springer, Dordrecht, the Netherlands, 2005.
- Calisto, M., Usoskin, I., Rozanov, E., and Peter, T.: Influence of Galactic Cosmic Rays on atmospheric composition and dynamics, *Atmos. Chem. Phys.*, 11, 4547–4556, <https://doi.org/10.5194/acp-11-4547-2011>, 2011.
- Damiani, A., Funke, B., López Puertas, M., Santee, M. L., Cordero, R. R., and Watanabe, S.: Energetic particle precipitation: A major driver of the ozone budget in the Antarctic upper stratosphere, *Geophys. Res. Lett.*, 43, 3554–3562, <https://doi.org/10.1002/2016GL068279>, 2016.
- Egorova, T., Rozanov, E., Zubov, V., and Karol, I.: Model for investigating ozone trends (MEZON), *Izv. Atmos. Ocean. Phys.*, 39, 277–292, 2003.
- Fischer, H., Birk, M., Blom, C., Carli, B., Carlotti, M., von Clarmann, T., Delbouille, L., Dudhia, A., Ehnhalt, D., Endemann, M., Flaud, J. M., Gessner, R., Kleinert, A., Koopman, R., Langen, J., López-Puertas, M., Mosner, P., Nett, H., Oelhaf, H., Perron, G., Remedios, J., Ridolfi, M., Stiller, G., and Zander, R.: MIPAS: an instrument for atmospheric and climate research, *Atmos. Chem. Phys.*, 8, 2151–2188, <https://doi.org/10.5194/acp-8-2151-2008>, 2008.
- Froidevaux, L., Jiang, Y. B., Lambert, A., Livesey, N. J., Read, W. G., Waters, J. W., Browell, E. V., Hair, J. W., Avery, M. A., McGee, T. J., Twigg, L. W., Sunnicht, G. K., Jucks, K. W., Margitan, J. J., Sen, B., Stachnik, R. A., Toon, G. C., Bernath, P. F., Boone, C. D., Walker, K. A., Filipiak, M. J., Harwood, R. S., Fuller, R. A., Manney, G. L., Schwartz, M. J., Daffer, W. H., Drouin, B. J., Cofield, R. E., Cuddy, D. T., Jarnot, R. F., Knosp, B. W., Perun, V. S., Snyder, W. V., Stek, P. C., Thurstans, R. P., and Wagner, P. A.: Validation of Aura Microwave Limb Sounder stratospheric ozone measurements, *J. Geophys. Res.-Atmos.*, 113, D15S20, <https://doi.org/10.1029/2007JD008771>, 2008.
- Funke, B., López-Puertas, M., Stiller, G. P., and von Clarmann, T.: Mesospheric and stratospheric NO<sub>y</sub> produced by energetic particle precipitation during 2002–2012, *J. Geophys. Res.-Atmos.*, 119, 4429–4446, <https://doi.org/10.1002/2013JD021404>, 2014.
- Funke, B., López-Puertas, M., Stiller, G. P., Versick, S., and von Clarmann, T.: A semi-empirical model for mesospheric and stratospheric NO<sub>y</sub> produced by energetic particle precipitation, *Atmos. Chem. Phys.*, 16, 8667–8693, <https://doi.org/10.5194/acp-16-8667-2016>, 2016.
- Fytterer, T., Mlynczak, M. G., Nieder, H., Pérot, K., Sinnhuber, M., Stiller, G., and Urban, J.: Energetic particle induced intra-seasonal variability of ozone inside the Antarctic polar vortex observed in satellite data, *Atmos. Chem. Phys.*, 15, 3327–3338, <https://doi.org/10.5194/acp-15-3327-2015>, 2015.
- Hitchcock, P., Shepherd, T. G., and Manney, G. L.: Statistical characterization of Arctic polar-night jet oscillation events, *J. Climate*, 26, 2096–2116, <https://doi.org/10.1175/JCLI-D-12-00202.1>, 2013.
- Jackman, C. H., Marsh, D. R., Vitt, F. M., Garcia, R. R., Fleming, E. L., Labow, G. J., Randall, C. E., López-Puertas, M., Funke, B., von Clarmann, T., and Stiller, G. P.: Short- and medium-term atmospheric constituent effects of very large solar proton events, *Atmos. Chem. Phys.*, 8, 765–785, <https://doi.org/10.5194/acp-8-765-2008>, 2008.
- Jungclaus, J. H., Keenlyside, N., Botzet, M., Haak, H., Luo, J. J., Latif, M., Marotzke, J., Mikolajewicz, U., and Roeckner, E.: Ocean circulation and tropical variability in the coupled model ECHAM5/MPI-OM, *J. Climate*, 19, 3952–3972, <https://doi.org/10.1175/JCLI3827.1>, 2006.
- Livesey, N. J., Read, W. G., Wagner, P. A., Froidevaux, L., Lambert, A., Manney, G. L., Millain, L. F., Pumphrey, Hugh, C., Santee, M. L., Schwartz, M. J., Wang, S., Fuller, R. A., Jarnot, R. F., Knosp, B. W., and Martinez, E.: Version 4.2x Level 2 data quality and description document. Earth Observing System (EOS) Aura Microwave Limb Sounder (MLS), available at: [https://mls.jpl.nasa.gov/data/v4-2\\_data\\_quality\\_document.pdf](https://mls.jpl.nasa.gov/data/v4-2_data_quality_document.pdf) (last access: 6 April 2019), 2018.
- Maliniemi, V., Asikainen, T., and Mursula, K.: Spatial distribution of Northern Hemisphere winter temperatures during different phases of the solar cycle, *J. Geophys. Res.-Atmos.*, 119, 9752–9764, <https://doi.org/10.1002/2013JD021343>, 2014.
- Marsh, D. R., Garcia, R. R., Kinnison, D. E., Boville, B. A., Sassi, F., Solomon, S. C., and Matthes, K.: Modeling the whole atmosphere response to solar cycle changes in radiative and geomagnetic forcing, *J. Geophys. Res.-Atmos.*, 112, 1–20, <https://doi.org/10.1029/2006JD008306>, 2007.
- Marsland, S. J., Haak, H., Jungclaus, J. H., Latif, M., and Röske, F.: The Max-Planck-Institute global ocean/sea ice model with orthogonal curvilinear coordinates, *Ocean Model.*, 5, 91–127, [https://doi.org/10.1016/S1463-5003\(02\)00015-X](https://doi.org/10.1016/S1463-5003(02)00015-X), 2002.
- Matthes, K., Funke, B., Andersson, M. E., Barnard, L., Beer, J., Charbonneau, P., Clilverd, M. A., Dudok de Wit, T., Haberer, M., Hendry, A., Jackman, C. H., Kretzschmar, M., Kruschke, T., Kunze, M., Langematz, U., Marsh, D. R., Maycock, A. C., Misios, S., Rodger, C. J., Scaife, A. A., Seppälä, A., Shangguan, M., Sinnhuber, M., Tourpali, K., Usoskin, I.,

- van de Kamp, M., Verronen, P. T., and Versick, S.: Solar forcing for CMIP6 (v3.2), *Geosci. Model Dev.*, 10, 2247–2302, <https://doi.org/10.5194/gmd-10-2247-2017>, 2017.
- Mironova, I. A., Aplin, K. L., Arnold, F., Bazilevskaya, G. A., Harrison, R. G., Krivolutsky, A. A., Nicoll, K. A., Rozanov, E. V., Turunen, E., and Usoskin, I. G.: Energetic Particle Influence on the Earth's Atmosphere, *Space Sci. Rev.*, 194, 1–96, <https://doi.org/10.1007/s11214-015-0185-4>, 2015.
- Muthers, S., Anet, J. G., Stenke, A., Raible, C. C., Rozanov, E., Brönnimann, S., Peter, T., Arfeuille, F. X., Shapiro, A. I., Beer, J., Steinhilber, F., Brugnara, Y., and Schmutz, W.: The coupled atmosphere–chemistry–ocean model SOCOL-MPIOM, *Geosci. Model Dev.*, 7, 2157–2179, <https://doi.org/10.5194/gmd-7-2157-2014>, 2014.
- Pierrard, V. and Lopez Rosson, G.: The effects of the big storm events in the first half of 2015 on the radiation belts observed by EPT/PROBA-V, *Ann. Geophys.*, 34, 75–84, <https://doi.org/10.5194/angeo-34-75-2016>, 2016.
- Reddmann, T., Ruhnke, R., Versick, S., and Kouker, W.: Modeling disturbed stratospheric chemistry during solar-induced NO<sub>x</sub> enhancements observed with MIPAS/ENVISAT, *J. Geophys. Res.*, 115, D00I11, <https://doi.org/10.1029/2009JD012569>, 2010.
- Roeckner, E. and Bäuml, G.: The Atmospheric General Circulation Model ECHAM5 Model description, *Max Plank Inst. Meteorol. Sci. Rep.*, 1–127, 2003.
- Rozanov, E., Calisto, M., Egorova, T., Peter, T., and Schmutz, W.: Influence of the Precipitating Energetic Particles on Atmospheric Chemistry and Climate, *Surv. Geophys.*, 33, 483–501, <https://doi.org/10.1007/s10712-012-9192-0>, 2012.
- Rozanov, E. V., Zubov, V. A., Schlesinger, M. E., Yang, F., and Andronova, N. G.: The UIUC three-dimensional stratospheric chemical transport model: Description and evaluation of the simulated source gases and ozone, *J. Geophys. Res.*, 104, 11755, <https://doi.org/10.1029/1999JD900138>, 1999.
- Schmidt, H., Brasseur, G. P., Charron, M., Manzini, E., Giorgetta, M. A., Diehl, T., Fomichev, V. I., Kinnison, D., Marsh, D., and Walters, S.: The HAMMONIA chemistry climate model: Sensitivity of the mesopause region to the 11-year solar cycle and CO<sub>2</sub> doubling, *J. Climate*, 19, 3903–3931, <https://doi.org/10.1175/JCLI3829.1>, 2006.
- Semeniuk, K., Fomichev, V. I., McConnell, J. C., Fu, C., Melo, S. M. L., and Usoskin, I. G.: Middle atmosphere response to the solar cycle in irradiance and ionizing particle precipitation, *Atmos. Chem. Phys.*, 11, 5045–5077, <https://doi.org/10.5194/acp-11-5045-2011>, 2011.
- Seppälä, A., Lu, H., Clilverd, M. A., and Rodger, C. J.: Geomagnetic activity signatures in wintertime stratosphere wind, temperature, and wave response, *J. Geophys. Res.-Atmos.*, 118, 2169–2183, <https://doi.org/10.1002/jgrd.50236>, 2013.
- Sheese, P. E., Walker, K. A., Boone, C. D., McLinden, C. A., Bernath, P. F., Bourassa, A. E., Burrows, J. P., Degenstein, D. A., Funke, B., Fussen, D., Manney, G. L., McElroy, C. T., Murtagh, D., Randall, C. E., Raspollini, P., Rozanov, A., Russell III, J. M., Suzuki, M., Shiotani, M., Urban, J., von Clarmann, T., and Zawodny, J. M.: Validation of ACE-FTS version 3.5 NO<sub>y</sub> species profiles using correlative satellite measurements, *Atmos. Meas. Tech.*, 9, 5781–5810, <https://doi.org/10.5194/amt-9-5781-2016>, 2016.
- Sinnhuber, M., Berger, U., Funke, B., Nieder, H., Reddmann, T., Stiller, G., Versick, S., von Clarmann, T., and Wissing, J. M.: NO<sub>y</sub> production, ozone loss and changes in net radiative heating due to energetic particle precipitation in 2002–2010, *Atmos. Chem. Phys.*, 18, 1115–1147, <https://doi.org/10.5194/acp-18-1115-2018>, 2018.
- Solomon, S., Crutzen, P. J., and Roble, R. G.: Photochemical coupling between the thermosphere and the lower atmosphere: 1. Odd nitrogen from 50 to 120 km, *J. Geophys. Res.*, 87, 7206, <https://doi.org/10.1029/JC087iC09p07206>, 1982.
- SPARC: The SPARC Data Initiative: Assessment of stratospheric trace gas and aerosol climatologies from satellite limb sounders, edited by: Hegglin, M. I. and Tegtmeier, S., SPARC Report No. 8, WCRP-05/2017, <https://doi.org/10.3929/ethz-a-010863911>, 2017.
- Stenke, A., Schraner, M., Rozanov, E., Egorova, T., Luo, B., and Peter, T.: The SOCOL version 3.0 chemistry–climate model: description, evaluation, and implications from an advanced transport algorithm, *Geosci. Model Dev.*, 6, 1407–1427, <https://doi.org/10.5194/gmd-6-1407-2013>, 2013.
- Turunen, E., Verronen, P. T., Seppälä, A., Rodger, C. J., Clilverd, M. A., Tamminen, J., Enell, C. F., and Ulich, T.: Impact of different energies of precipitating particles on NO<sub>x</sub> generation in the middle and upper atmosphere during geomagnetic storms, *J. Atmos. Sol.-Terr. Phys.*, 71, 1176–1189, <https://doi.org/10.1016/j.jastp.2008.07.005>, 2009.
- Verronen, P. T. and Lehmann, R.: Enhancement of odd nitrogen modifies mesospheric ozone chemistry during polar winter, *Geophys. Res. Lett.*, 42, 10445–10452, <https://doi.org/10.1002/2015GL066703>, 2015.
- Waters, J. W., Froidevaux, L., Harwood, R. S., Jarnot, R. F., Pickert, H. M., Read, W. G., Siegel, P. H., Cofield, R. E., Filipiak, M. J., Flower, D. A., Holden, J. R., Lau, G. K., Livesey, N. J., Manney, G. L., Pumphrey, H. C., Santee, M. L., Wu, D. L., Cuddy, D. T., Lay, R. R., Loo, M. S., Perun, V. S., Schwartz, M. J., Stek, P. C., Thurstans, R. P., Boyles, M. A., Chandra, K. M., Chavez, M. C., Chen, G. S., Chudasama, B. V., Dodge, R., Fuller, R. A., Girard, M. A., Jiang, J. H., Jiang, Y., Knosp, B. W., Labelle, R. C., Lam, J. C., Lee, K. A., Miller, D., Oswald, J. E., Patel, N. C., Pukala, D. M., Quintero, O., Scaff, D. M., Van Snyder, W., Tope, M. C., Wagner, P. A., and Walch, M. J.: The Earth Observing System Microwave Limb Sounder (EOS MLS) on the aura satellite, *IEEE T. Geosci. Remote*, 44, 1075–1092, <https://doi.org/10.1109/TGRS.2006.873771>, 2006.
- Wissing, J. M. and Kallenrode, M. B.: Atmospheric ionization module Osnabrück (AIMOS): A 3-D model to determine atmospheric ionization by energetic charged particles from different populations, *J. Geophys. Res.-Space*, 114, 1–14, <https://doi.org/10.1029/2008JA013884>, 2009.
- Yando, K., Millan, R. M., Green, J. C., and Evans, D. S.: A Monte Carlo simulation of the NOAA POES Medium Energy Proton and Electron Detector instrument, *J. Geophys. Res.-Space*, 116, 1–13, <https://doi.org/10.1029/2011JA016671>, 2011.